

# Upper Bound on the Modal Material Loss Rate in Plasmonic and Metamaterial Systems

Aaswath Raman\*

*Department of Applied Physics, Stanford University, Stanford, California 94305, USA*

Wonseok Shin and Shanhui Fan†

*Department of Electrical Engineering, Stanford University, Stanford, California 94305, USA*  
(Received 4 October 2012; revised manuscript received 15 January 2013; published 29 April 2013)

A better understanding of optical loss in plasmonic and metamaterial systems is of increasing importance for both basic and applied research in a broad range of topics including sensors, antennas, optical interconnects, and photovoltaics. In this Letter, we use a photonic band formalism for plasmonics to exactly derive a fundamental upper bound on the nonradiative material loss rate of modes in plasmonic, polaritonic, and metamaterial systems. This bound is purely defined by material properties and cannot be overcome by device design. Moreover it is frequency dependent in the presence of multiple Lorentz poles. We numerically verify this bound through direct calculations for a range of plasmonic systems, including optical antennas where the bound places fundamental performance constraints.

DOI: [10.1103/PhysRevLett.110.183901](https://doi.org/10.1103/PhysRevLett.110.183901)

PACS numbers: 41.20.-q, 42.70.Qs, 71.45.Gm, 78.67.Pt

Understanding optical loss in plasmonic, polaritonic, and metamaterial systems is of fundamental importance to continued progress in photonics research. The coupling of photons to the electrons in the metal is at the origin of deep subwavelength modal confinement, and also results in a powerful absorption and loss mechanism for electromagnetic modes in such metallic systems. This optical loss and absorption can be a limiting factor for some applications [1–8]. On the other hand, enhanced optical loss in plasmonic systems has recently been leveraged to improve and maximize absorption for a range of applications [9] including ultrathin absorbers [10] and photodetectors [11].

In this Letter, we prove rigorously that, for any electromagnetic mode of a plasmonic structure, there exists an upper bound on its material loss rate. When the plasmonic material is described by a multipole Lorentz model, the upper bound is a frequency-dependent weighted average of the damping rates of the oscillators that underlie the poles. We validate this proof by full-field simulations of a variety of systems including periodic arrays of slot antennas.

There have been numerous numerical studies of the loss properties of plasmonic structures [5,12–18]. The calculation of the modal material loss rate has also been used to understand the effect of plasmonic loss in solar cell light trapping schemes [19]. However, only a few recent papers have attempted to understand the general behavior of loss in plasmonic systems from a purely analytic perspective. Wang and Shen showed that in the quasistatic limit the intrinsic  $Q$  is fixed by the material used and resonance frequency considered, and argued that it would be difficult to do better than their prediction [20]. Their derivation also assumes a form of energy density that is accurate only in the low-loss limit, further limiting the applicability of their results. Khurgin and Sun have presented a scaling analysis of loss with respect to size and wavelength, in particular

related to nanoparticles and split-ring resonators [21]. In contrast to these works, we are not restricted to the quasi-static limit, any specific geometry or the Drude model. Our analysis is fully analytic and rigorous, derived directly from Maxwell's equations and for material systems described by an arbitrary number of lossy Lorentz poles.

We begin by considering materials whose permittivities can be described by

$$\varepsilon(\omega) = \varepsilon_\infty + \varepsilon_\infty \sum_{n=1}^N \frac{\omega_{p,n}^2}{\omega_{0,n}^2 - \omega^2 + i\omega\Gamma_n}. \quad (1)$$

This is the standard  $N$ -pole Lorentz-Drude function widely used to fit the permittivities of dispersive materials such as metals [22] or polaritonic materials such as SiC. As a shorthand, we refer to all such materials as metals in the rest of the Letter but emphasize that these results extend to any material system whose dielectric function can be described by Lorentz poles. The  $n$ th pole is characterized by its resonance frequency  $\omega_{0,n}$ , its damping rate  $\Gamma_n$ , and its oscillator strength  $\omega_{p,n}$ . For many metals in the optical wavelength range, it is essential to use multiple poles in order to capture contributions to the permittivities from both intraband, and interband transitions. The intraband transition gives rise to free-electron behavior that is characterized by a Drude pole with its resonance frequency  $\omega_0 = 0$ , whereas the interband transition gives rise to a Lorentz pole.

We also note here the Thomas-Reiche-Kuhn sum rule [23]  $\sum_{n=1}^N \omega_{p,n}^2 = n_e e^2 / m \varepsilon_\infty \equiv \omega_p^2$  where  $e$  and  $m$  are the charge and effective mass of electrons, respectively. The sum rule limits the total strength of the poles by  $n_e$ , the number density of electrons relevant to transitions in the frequency range of interest. The effect of higher-frequency transitions related to core electrons in the material can be

captured by the  $\varepsilon_\infty$  term (see Supplemental Material [24]). Thus, we can express the oscillator strength of each pole as  $\omega_{p,n}^2 = f_n \omega_p^2$  where  $\sum_{n=1}^N f_n = 1$ .

For the steady state, with fields varying as  $\exp(i\omega t)$ , the dispersive material characterized by Eq. (1) can be described by the following equations [25,26]:

$$i\omega \mathbf{H} = -\frac{1}{\mu_0} \nabla \times \mathbf{E}, \quad (2)$$

$$i\omega \mathbf{E} = \frac{1}{\varepsilon_\infty} \left( \nabla \times \mathbf{H} - \sum_{n=1}^N \mathbf{V}_n \right), \quad (3)$$

$$i\omega \mathbf{P}_n = \mathbf{V}_n, \quad (4)$$

$$i\omega \mathbf{V}_n = f_n \omega_p^2 \varepsilon_\infty \mathbf{E} - \omega_{0,n}^2 \mathbf{P}_n - \Gamma_n \mathbf{V}_n. \quad (5)$$

Here for the  $n$ th pole in Eq. (1), we introduce auxiliary mechanical fields  $\mathbf{P}_n$  and  $\mathbf{V}_n$  that describe the position and velocity of the corresponding electronic oscillator. Equations (2) and (3) also define a total energy density for the given oscillator model

$$W_0 = \frac{1}{4} (\varepsilon_\infty |\mathbf{E}|^2 + \mu_0 |\mathbf{H}|^2) + \sum_{n=1}^N \frac{1}{4f_n \omega_p^2 \varepsilon_\infty} (\omega_{0,n}^2 |\mathbf{P}_n|^2 + |\mathbf{V}_n|^2). \quad (6)$$

The  $\sum_{n=1}^N \frac{1}{4f_n \omega_p^2 \varepsilon_\infty} |\mathbf{V}_n|^2$  term corresponds to the kinetic energy of the electrons. We note that this kinetic energy is used to determine the kinetic inductance term in *RLC*-circuit models of metamaterials [27].

Solving the eigenvalue problem defined by Eqs. (2)–(5) results in eigenfrequencies  $\omega = \omega_r + i\gamma$  that are complex in general, with  $\omega_r$  corresponding to the modal frequency and  $\gamma$  the mode's material loss rate. Below we will use Eqs. (2)–(5) to constrain the behavior of the modal material loss rate  $\gamma$ .

From Eqs. (2)–(5) we obtain

$$\begin{aligned} (\omega_r + i\gamma) & \left[ \mu_0 \mathbf{H}^* \cdot \mathbf{H} + \sum_{n=1}^N \frac{1}{f_n \omega_p^2 \varepsilon_\infty} \mathbf{V}_n^* \cdot \mathbf{V}_n \right] \\ & - \sum_{n=1}^N \frac{i\Gamma_n}{f_n \omega_p^2 \varepsilon_\infty} \mathbf{V}_n^* \cdot \mathbf{V}_n \\ & = (\omega_r - i\gamma) \left[ \varepsilon_\infty \mathbf{E}^* \cdot \mathbf{E} + \sum_{n=1}^N \frac{\omega_{0,n}^2}{f_n \omega_p^2 \varepsilon_\infty} \mathbf{P}_n^* \cdot \mathbf{P}_n \right] \\ & + i[\mathbf{H}^* \cdot (\nabla \times \mathbf{E}) - \mathbf{E} \cdot (\nabla \times \mathbf{H}^*)]. \end{aligned} \quad (7)$$

We integrate both sides of Eq. (7) over space. We use the standard vector field identity on the last term of Eq. (7) and find a  $\int d\mathbf{r} \nabla \cdot (\mathbf{E} \times \mathbf{H}^*)$  term. For closed or periodic systems this term is zero, and in practice it is  $\approx 0$  for many open systems of interest where the field is strongly

confined to a metal-dielectric interface. We then separate the real and imaginary components of Eq. (7) respectively to find the first result of the Letter

$$\begin{aligned} \int d\mathbf{r} & \left( \mu_0 |\mathbf{H}|^2 + \sum_{n=1}^N \frac{1}{f_n \omega_p^2 \varepsilon_\infty} |\mathbf{V}_n|^2 \right) \\ & = \int d\mathbf{r} \left( \varepsilon_\infty |\mathbf{E}|^2 + \sum_{n=1}^N \frac{\omega_{0,n}^2}{f_n \omega_p^2 \varepsilon_\infty} |\mathbf{P}_n|^2 \right), \end{aligned} \quad (8)$$

and

$$\gamma = \frac{\int d\mathbf{r} \sum_{n=1}^N (\Gamma_n / 4f_n \omega_p^2 \varepsilon_\infty) |\mathbf{V}_n|^2}{\int d\mathbf{r} W_0}. \quad (9)$$

We emphasize that both Eq. (8) and (9) are *exact* for closed and periodic systems, and in practice accurately describe many open plasmonic systems of interest. Equation (8) states that, for a given mode, the sum of the magnetic energy and kinetic energy of the electrons is equal to the sum of the electric energy and potential energy of the electrons. Equation (9) relates the modal material loss rate to the fraction of its total energy that is in the kinetic energy of the electrons. A formula regarding loss reminiscent of Eq. (9) was previously derived in Ref. [25] using first-order perturbation theory, starting from the mode of a fictitious lossless system. In contrast, the result here, with the fields being the actual modal fields of the lossy system, is much stronger: it has no approximation and does not rely upon perturbation theory.

Comparing Eqs. (6) and (8) straightforwardly leads to an exact bound on the kinetic energy of the electrons that is quantified by the  $\mathbf{V}$  field:

$$\int d\mathbf{r} \sum_{n=1}^N \frac{1}{4f_n \omega_p^2 \varepsilon_\infty} |\mathbf{V}_n|^2 \leq \int d\mathbf{r} \frac{1}{2} W_0. \quad (10)$$

Combining Eq. (10) and (9) (see Supplemental Material [24]) we obtain our second main result, an expression for  $\gamma_{\max}$ , the upper bound on the material loss rate of every mode of the system

$$\gamma \leq \gamma_{\max}(\omega_r) = \sum_{n=1}^N \theta_n(\omega_r) \frac{\Gamma_n}{2}, \quad (11)$$

where

$$\theta_n(\omega_r) = \frac{f_n / [(\omega_{0,n}^2 - \omega_r^2)^2 + \omega_r^2 \Gamma_n^2]}{\sum_{n=1}^N f_n / [(\omega_{0,n}^2 - \omega_r^2)^2 + \omega_r^2 \Gamma_n^2]}. \quad (12)$$

$\theta_n(\omega_r)$  are frequency-dependent weighting factors such that  $\sum_{n=1}^N \theta_n(\omega_r) = 1$ . This expression is an approximation derived in the limit that  $\gamma \ll \omega_r$  which corresponds to most plasmonic situations of interest. More generally, the upper bound can also be expressed as an exact, self-consistent equation for  $\gamma_{\max}$  (see Supplemental Material [24]). The upper bound  $\gamma_{\max}(\omega_r)$  is thus a frequency-dependent weighted average of one-half the damping rates

of the poles,  $\Gamma_n/2$ . The weighting takes into account both the strength of the damping and the strength of the pole itself. Thus a weak pole (small  $f_n$ ) has limited effect on the upper bound even if it has an extremely large corresponding damping rate  $\Gamma_n$ . The behavior of the upper bound is thus complex and depends on the distributions of pole parameters for a material. As such, the maximum upper bound over all frequencies will not necessarily be  $\max(\Gamma_n)/2$  and, as we show in the numerical results, it can be substantially lower than this value.

To further examine the implications of Eqs. (11) and (12) we consider a few special cases that are of practical interest: (1) Single-pole case: The upper bound is exactly  $\gamma_{\max} = \Gamma_1/2$  for all frequencies. (2) Multipole case: Suppose there exists a  $k$ th pole with its frequency far away from other poles such that  $\theta_k(\omega_r) \gg \theta_n(\omega_r)$ ,  $n \neq k$ . Near this  $k$ th pole then we have  $\gamma_{\max} \approx \frac{1}{2}\Gamma_k$ . This is particularly relevant when one has a Drude term as characterised by a resonance frequency  $\omega_0 = 0$  and a damping rate  $\Gamma_{\text{Drude}}$ . In such cases, the Drude damping rate dominates for low frequencies away from the lowest frequency Lorentz pole and  $\gamma_{\max} \approx \Gamma_{\text{Drude}}/2$ . (3) High-frequency limit: The upper bound in this case is a constant sum of the damping rates of the oscillators weighted by the strength of each oscillator:

$$\gamma_{\max}(\omega_r \rightarrow \infty) = \sum_{n=1}^N f_n \Gamma_n. \quad (13)$$

The upper bound on  $\gamma$  corresponds to a lower bound on the intrinsic quality factor  $Q_i \geq \omega_r/2\gamma_{\max}(\omega_r)$ . We note finally that both these bounds are purely dependent on material properties and cannot be overcome by varying a plasmonic nanostructure's shape or design. Moreover, as we show in the numerical examples below, plasmonic modes with electromagnetic fields confined to deep sub-wavelength regions are often very close to this limit.

We now numerically verify this result. For direct verification we calculate  $\gamma$  for the eigenmodes of a variety of plasmonic nanostructures either analytically or numerically using the method of Ref. [25]. First, for simplicity, we use a  $N = 1$  Drude fit of silver where  $\epsilon_\infty = \epsilon_0$ ,  $\omega_0 = 0$ ,  $\omega_p = 2\pi c/a$ , and  $\Gamma = 0.0025\omega_p$  for  $a = 136$  nm. We begin with a simple metal-air interface and calculate  $\gamma$  analytically (see Supplemental Material [24]) for the fundamental surface plasmon mode. As shown in Fig. 1,  $\gamma$  indeed saturates at  $\gamma_{\max} = \Gamma/2$  as  $k_x \rightarrow \infty$ . For a metal-air interface this corresponds to  $\omega_r \rightarrow \omega_p/\sqrt{2} \equiv \omega_{sp}$ , the surface plasmon frequency.

Next we consider a more complex plasmonic nanostructure consisting of a 2D periodic array of silver slot antennas in air. For the plasmonic material we use a  $N = 3$  fit of silver (see Supplemental Material [24], Table I). We plot the corresponding  $\gamma_{\max}(\omega_r)$  in Fig. 2(a). In consistency with case (2) of the theory presented earlier, we observe that in the frequency region near a pole  $\gamma_{\max}(\omega_r)$  is dominated by the damping rate of such a pole. In frequency

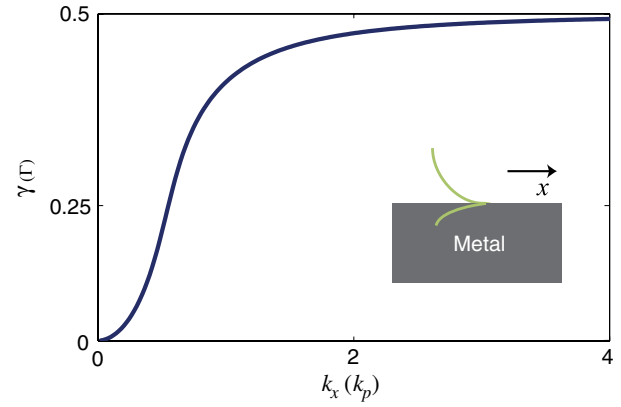


FIG. 1 (color online). Modal material loss rate ( $\gamma$  in units of  $\Gamma$ ) vs wave vector ( $k_x$  in units of  $k_p$ ) for a planar metal-air interface calculated analytically. The metal is described by  $\epsilon(\omega) = 1 - \omega_p^2/\omega(\omega - i\Gamma)$ , and  $k_p = \omega_p/c$ .  $\gamma$  approaches  $\gamma_{\max} = \Gamma/2$  for large  $k_x$ , where the field is strongly confined spatially to the interface.

regions between poles,  $\gamma_{\max}(\omega_r)$  is a weighted average of the damping rates of the poles. Furthermore, in this example the maximum of the upper bound is in fact lower than the largest damping rate,  $\Gamma_3/2$ , due to the complex interaction of the strengths and damping terms of these three Lorentz poles.

Having discussed the upper bound of the modal material loss rate, which is determined by the plasmonic material model only, we now consider the material loss rate of the optical modes of the antenna array. We calculate  $\gamma$  of transverse-electric ( $E_x$  and  $E_y$  in-plane) modes for all wave vectors  $k$  in the irreducible first

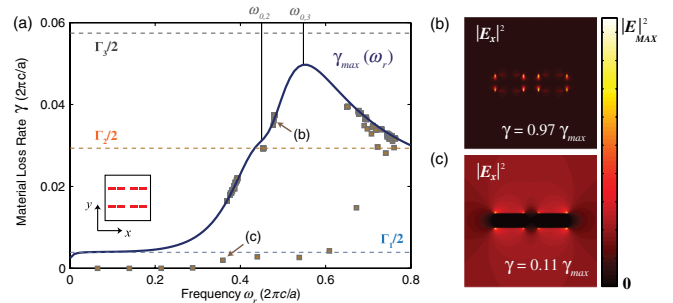


FIG. 2 (color online). (a) Modal material loss rate ( $\gamma$  in units of  $2\pi c/a$ , where  $a = 136$  nm is the period) vs real frequency ( $\omega_r$  in units of  $2\pi c/a$ ) for all transverse-electric modes of a 2D periodic array of plasmonic slot antennas (shown in the inset) in the first Brillouin zone. The plasmonic material is described by a three-pole fit of silver's dielectric function described in Table I in the Supplemental Material [24]. The  $\gamma$  values, numerically calculated via the method of Ref. [25], are shown as individual points. Many modes follow the upper bound  $\gamma_{\max}$  (marked by the blue line) but do not exceed it. (b), (c) Electric field intensity ( $|E_x|^2$ ) of two eigenmodes with large and small  $\gamma$ . The modes with larger  $\gamma$  that approach  $\gamma_{\max}$  exhibit field profiles that are strongly concentrated along the metal-air interfaces of the antenna.

Brillouin zone. These  $\gamma$  are plotted against their corresponding real frequency  $\omega_r$  in Fig. 2(a) as squares. As in Fig. 1 the numerically calculated  $\gamma$  for the antenna array's optical modes do not exceed the predicted upper bound of  $\gamma_{\max}(\omega_r)$ , but many modes do approach this bound. We compare two modes with large and small  $\gamma$  in Figs. 2(b) and 2(c), respectively. The eigenmode with strong field confinement [Fig. 2(b)] at the metal-air interface has a large  $\gamma$ , approaching the limit of  $\gamma_{\max}$ . Similar behavior is also seen in the case of plasmonic cavities (see numerical example in the Supplemental Material [24]). Through these numerical examples, we have demonstrated that the upper bound as derived theoretically can indeed be used to constrain modal loss behavior in plasmonic structures in a general multipole, multiple mode situation.

We now demonstrate how our rigorous understanding of the modal material loss rate of plasmonic modes sheds light on general behaviors of optical antennas [7,8]. In 2D, a deep subwavelength lossless optical antenna ( $\Gamma = 0$ ) that supports a single resonance has a scattering cross section  $C_{\text{lossless}}$  [28]

$$C_{\text{lossless}} = \frac{2\lambda}{\pi} \frac{\eta^2}{(\omega_r - \Omega)^2 + \eta^2}. \quad (14)$$

Here  $\Omega$  is the resonance frequency,  $\eta$  is the external linewidth due to the antenna's radiation. In the lossless system, the external linewidth exclusively defines the total linewidth and the total quality factor  $Q$ . A lossy version of the same antenna has a scattering cross section  $C_{\text{lossy}}$  defined as

$$C_{\text{lossy}} = \frac{2\lambda}{\pi} \frac{\eta^2}{(\omega_r - \Omega)^2 + (\eta + \gamma)^2}. \quad (15)$$

For the lossy antenna, the total linewidth is the sum of the external linewidth  $\eta$  due to radiation, and the modal material loss rate  $\gamma$ , which is sometimes also referred to as the intrinsic linewidth. Our theory constrains this  $\gamma$  and hence constrains the antenna behavior.

As a concrete example, we consider five rectangular plasmonic antenna structures [inset, Fig. 3(a)]. These antenna structures are made of gold, defined by a  $N = 1$  fit of Eq. (1) where  $\omega_0 = 0$ ,  $\omega_p = 4.12 \times 10^{15} \text{ s}^{-1}$ ,  $\epsilon_\infty = 11\epsilon_0$  and  $\Gamma = 4.12 \times 10^{13} \text{ s}^{-1}$ . All antenna structures have a constant aspect ratio, with the largest being  $80 \text{ nm} \times 16 \text{ nm}$ , and the smallest  $10 \text{ nm} \times 2 \text{ nm}$ .

We simulate these antenna structures using the finite-difference frequency-domain method [29]. The finite-difference grid used in the simulation has a spatial resolution that varies from  $1.33 \text{ nm}$  for the largest antenna to  $0.167 \text{ nm}$  for the smallest antenna. These resolutions were chosen since higher grid resolution resulted in no substantial changes in the field patterns and resonances observed. We calculate the scattering cross sections of these antennas using the total-field-scattered-field method [30]. For each antenna structure we calculate its scattering

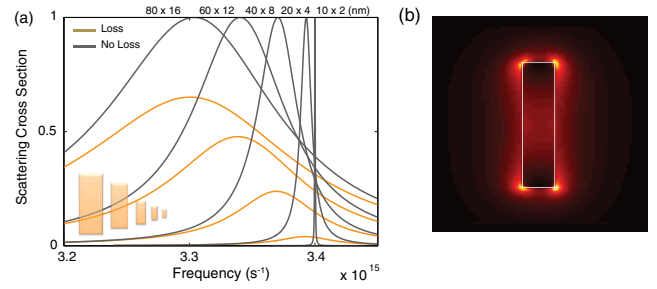


FIG. 3 (color online). (a) Normalized scattering cross sections for 2D lossless and lossy gold dipole antennas of varying dimensions (aspect ratio maintained). Smaller antennas have higher resonance frequencies and the lossy antennas have smaller scattering cross sections compared with its lossless counterpart. (b) Electric field intensity for the  $60 \times 12 \text{ nm}$  antenna at resonance as solved by the finite-difference frequency-domain method.

cross section, both for the lossy case with full material loss, and for the lossless case with  $\Gamma$  set to zero. The scattering cross-section spectra thus obtained for the five antenna structures are shown in Fig. 3(a). The modal field distribution at one of the resonance peaks is shown in Fig. 3(b) indicating that this is a half-wavelength antenna structure. We see that in reducing the antennas dimension its resonance frequencies shift to higher frequencies.

From the scattering cross-section spectra we extract the material loss and external radiation rates of these antenna structures. We fit Eq. (14) to the spectrum of the lossless case to determine the external radiation rate  $\eta$ . With  $\eta$  determined we then fit Eq. (15) to the lossy case to determine the modal material loss rate  $\gamma$ , as well as the intrinsic quality factor  $Q_i = \omega_r/2\gamma$ , where  $\omega_r$  is the resonance frequency.

We now plot the modal material loss rate for these five antenna structures, and the intrinsic quality factor of the resonance, as a function of resonance frequency (Fig. 4).

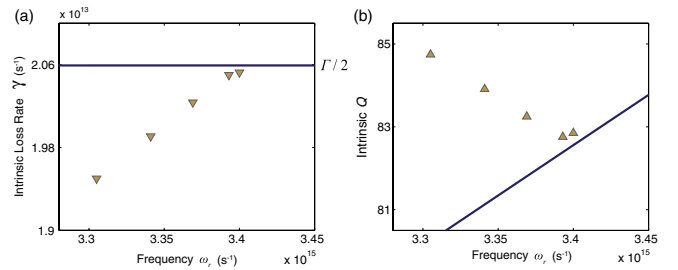


FIG. 4 (color online). (a) Modal material loss rates  $\gamma$  for the five plasmonic half-wavelength antennas shown in Fig. 3 as a function of their resonance frequency  $\omega_r$ . These loss rates approach the  $\gamma_{\max} = \Gamma/2$  limit (blue line) as  $\omega_r$  gets larger but do not exceed the upper bound. (b) Intrinsic  $Q$ -factor  $Q_i$  for the same antennas. The  $Q_i$  stay above the lower bound (blue line) of  $\omega_r/\Gamma$  and decrease with increasing  $\omega_r$  until they approach the bound line, and antennas at higher  $\omega_r$  can have higher  $Q_i$ .

We observe that the modal material loss rates  $\gamma$  all fall below  $\gamma_{\max} = \Gamma/2$  in Fig. 4(a), while the intrinsic quality factor  $Q_i$  are above  $\omega_r/\Gamma$  in Fig. 4(b), as expected from our theory. As the antennas become smaller, increasing their resonance frequencies, their  $\gamma$  increase while their  $Q_i$  decrease in value. This behavior persists until the  $\gamma$  values approach the upper bound of  $\gamma_{\max}$ . After this point smaller antennas operating with higher resonance frequencies  $\omega_r$  can have higher  $Q_i$  since their  $\gamma$  values have saturated near  $\gamma_{\max}$ . This effect, of a higher  $Q_i$  at higher resonance frequencies, is related to the assumption that the damping rates of the oscillators  $\Gamma_n$  is independent of the geometry. In practice, as the antenna becomes smaller,  $\Gamma_n$  will increase due to the finite-size effect, in which case the corresponding upper bound on the loss rate will depend on the antenna's size [31]. However, the general trend, that as the size of the antenna decreases, the actual modal material loss rate approaches its upper bound, remains valid. The trend that we observe here is consistent with previous works on metallic nanoparticles [28]. Finally, we note that this result is of practical relevance for the design of dark-state plasmonic antennas [5,32–35] where the resonance linewidth of the dark state is predominantly defined by its modal material loss rate.

In conclusion, we have analytically derived an exact energy relation between the electromagnetic fields and the mechanical motion of electrons in dispersive plasmonic and metamaterial systems. We have used this relation to place an upper bound on the material loss rate of optical modes in such dispersive systems, and verified this result numerically. These results were derived exactly without electrostatic approximations and apply generally to electromagnetic modes in any dispersive material system, including polaritonic materials. We believe these results offer a general framework to understand the modal material loss rates and linewidths of resonances in all plasmonic and metamaterial systems, and show that no amount of design can overcome material properties when it comes to the upper bound of the linewidth and corresponding lower bound on  $Q_i$ .

This work is supported by the Department of Energy Grant No. DE-FG02-07ER46426 and by an AFOSR-MURI program (FA9550-12-1-0471). A. R. acknowledges the support of Alberta Scholarship Programs' Sir James Loughheed Award of Distinction. W. S. acknowledges the support of Samsung Scholarship Foundation.

\*aaswath@stanford.edu

†shanhui@stanford.edu

- [1] E. Ozbay, *Science* **311**, 189 (2006).
- [2] H. A. Atwater and A. Polman, *Nat. Mater.* **9**, 205 (2010).
- [3] A. Boltasseva and H. A. Atwater, *Science* **331**, 290 (2011).
- [4] V. J. Sorger, R. F. Oulton, J. Yao, G. Bartal, and X. Zhang, *Nano Lett.* **9**, 3489 (2009).
- [5] N. J. Halas, S. Lal, W.-S. Chang, S. Link, and P. Nordlander, *Chem. Rev.* **111**, 3913 (2011).
- [6] Z. Ruan, M. Yan, C. W. Neff, and M. Qiu, *Phys. Rev. Lett.* **99**, 113903 (2007).
- [7] L. Novotny, *Phys. Rev. Lett.* **98**, 266802 (2007).
- [8] M. L. Brongersma, *Nat. Photonics* **2**, 270 (2008).
- [9] G. Veronis, R. W. Dutton, and S. Fan, *J. Appl. Phys.* **97**, 093104 (2005).
- [10] K. Aydin, V. E. Ferry, R. M. Briggs, and H. A. Atwater, *Nat. Commun.* **2**, 517 (2011).
- [11] M. W. Knight, H. Sobhani, P. Nordlander, and N. J. Halas, *Science* **332**, 702 (2011).
- [12] S. Zhang, W. Fan, K. J. Malloy, S. R. J. Brueck, N. C. Panou, and R. M. Osgood, *Opt. Express* **13**, 4922 (2005).
- [13] G. Dolling, M. Wegener, C. M. Soukoulis, and S. Linden, *Opt. Express* **15**, 11 536 (2007).
- [14] R. F. Oulton, G. Bartal, D. F. P. Pile, and X. Zhang, *New J. Phys.* **10**, 105018 (2008).
- [15] W. Cai, J. S. White, and M. L. Brongersma, *Nano Lett.* **9**, 4403 (2009).
- [16] J. B. Khurgin and G. Sun, *Appl. Phys. Lett.* **96**, 181102 (2010).
- [17] V. E. Ferry, J. N. Munday, and H. A. Atwater, *Adv. Mater.* **22**, 4794 (2010).
- [18] W. Shin, A. Raman, and S. Fan, *J. Opt. Soc. Am. B* **29**, 1048 (2012).
- [19] E. A. Schiff, *J. Appl. Phys.* **110**, 104501 (2012).
- [20] F. Wang and Y. R. Shen, *Phys. Rev. Lett.* **97**, 206806 (2006).
- [21] J. B. Khurgin and G. Sun, *Appl. Phys. Lett.* **99**, 211106 (2011).
- [22] A. D. Rakić, A. B. Djurišić, J. M. Elazar, and M. L. Majewski, *Appl. Opt.* **37**, 5271 (1998).
- [23] H. A. Bethe and E. E. Salpeter, *Quantum Mechanics of One- and Two-Electron Atoms* (Springer-Verlag, Berlin, 1957).
- [24] See Supplemental Material at <http://link.aps.org/supplemental/10.1103/PhysRevLett.110.183901> for derivation details, material parameters, and an additional numerical example.
- [25] A. Raman and S. Fan, *Phys. Rev. Lett.* **104**, 087401 (2010).
- [26] A. Raman and S. Fan, *Phys. Rev. B* **83**, 205131 (2011).
- [27] J. Zhou, T. Koschny, M. Kafesaki, E. N. Economou, J. B. Pendry, and C. M. Soukoulis, *Phys. Rev. Lett.* **95**, 223902 (2005).
- [28] C. F. Bohren and D. R. Huffman, *Absorption and Scattering of Light by Small Particles* (Wiley-Vch, New York, 2008).
- [29] W. Shin and S. Fan, *J. Comput. Phys.* **231**, 3406 (2012).
- [30] A. Taflov and S. C. Hagness, *Computational Electrodynamics: The Finite-Difference Time-Domain Method* (Artech House Publishers, Norwood, MA, 2005), 3rd ed.
- [31] E. S. Kooij and B. Poelsema, *Phys. Chem. Chem. Phys.* **8**, 3349 (2006).
- [32] L. Verslegers, Z. Yu, Z. Ruan, P. B. Catrysse, and S. Fan, *Phys. Rev. Lett.* **108**, 083902 (2012).
- [33] S. Zhang, D. A. Genov, Y. Wang, M. Liu, and X. Zhang, *Phys. Rev. Lett.* **101**, 047401 (2008).
- [34] N. Liu, L. Langguth, T. Weiss, J. Kästel, M. Fleischhauer, T. Pfau, and H. Giessen, *Nat. Mater.* **8**, 758 (2009).
- [35] R. Taubert, M. Hentschel, J. Kstel, and H. Giessen, *Nano Lett.* **12**, 1367 (2012).